Available online at www.sciencedirect.com
SCIENCE DIRECT®
Applied Catalysis B: Environmental 54 (2004) 145–154
APPLIED CATALYSIS B: ENVIRONMENTAL
www.elsevier.com/locate/apcatb

Uranyl-anchored MCM-41 as a highly efficient photocatalyst for the complete oxidation of methanol under sunlight

K. Vidya[a], V.S. Kamble[b], P. Selvam[a,*], N.M. Gupta[b]

[a]*Department of Chemistry, Indian Institute of Technology – Bombay, Powai, Mumbai 400076, India*
[b]*Applied Chemistry Division, Bhabha Atomic Research Centre, Trombay, Mumbai 400085, India*

Received 10 May 2004; accepted 2 July 2004
Available online 6 August 2004

Abstract

A photocatalyst that may exhibit high activity for oxidation of volatile organic compounds (VOCs) under solar radiation would offer a practical and economic means for the cleaning of air under environmental conditions. We report here for the first time that the uranyl ions anchored within the mesopores of MCM-41 may serve as an efficient heterogeneous photocatalyst for the complete destruction of methanol in vapor phase, and in the presence of sunlight and air. The uranyl-anchored MCM-41 was found to be more efficient than a TiO_2 photocatalyst in terms of $CH_3OH \rightarrow CO_2$ conversion rates. The reversible and active participation of uranyl groups in the studied photocatalytic reaction was ascertained with the help of in situ fluorescence and electron paramagnetic resonance techniques, whereas the radiation-induced transient species over catalyst surface were monitored using in situ FTIR spectroscopy. The detailed reaction mechanism and the role played by uranyl ions in the photooxidation of methanol over UO_2^{2+}/MCM are elucidated on the basis of these results.

Keywords: Photocatalytic oxidation; Uranyl ions; Sunlight; Methanol; VOCs

1. Introduction

The uranyl ions are known to possess distinctive photo-absorption, excitation, and emission characteristics, as compared to any other inorganic cation [1]. The lowest excited eigenvalue of the uranyl ion ($^*UO_2^{2+}$) is a strongly oxidizing species (E° = 2.6 V), which is found to be quenched by a variety of organic substrates resulting in the abstraction of their hydrogen atoms [2,3]. In view of this, a number of studies have utilized uranyl ions for homo-geneous- phase photooxidation reactions of hydrocarbons [4–9], chlorophenols [10], and substituted phenols [11], etc. Comparatively, fewer studies have been devoted to the photocatalytic activity of UO_2^{2+} ions in the heterogeneous reaction mode. For instance, Suib and co-workers [12–14] employed uranyl-exchanged clays and zeolites for the photooxidation of ethanol, isopropyl alcohol, and diethyl ether to yield the corresponding aldehydes and ketones. In another study, Dai et al. [15] reported the photocatalytic oxidation of ethanol solution by UO_2^{2+} doped glass, which resulted in the formation of acetaldehyde. These studies have demonstrated that the restricted pore dimensions of the zeolites and pillared clays may help in the controlled product selectivity. We may, however, point out that most of these works relate to the measurements performed in solution phase, and to the best of our knowledge, no studies have been reported so far on the vapor-phase photooxidation reactions of organic compounds utilizing uranyl ions as heterogeneous catalyst.

In our earlier publications [16–20], we have reported different methods of anchoring uranyl ions within the silicate matrix of mesoporous MCM-41 and MCM-48 hosts. The anchored UO_2^{2+} groups were found to be thermally stable, and only a small fraction was converted to nanosize crystallites of α-U_3O_8 after calcination at temperatures up to 800 °C. Furthermore, the entrapped UO_X moieties were found to exhibit excellent catalytic activity for the oxidation of various

* Corresponding author. Tel.: +91-22-2576-7155/2550-5146; fax: +91-22-2572-3480/2550-5151.
E-mail addresses: selvam@iitb.ac.in (P. Selvam), nmgupta@magnum.barc.ernet.in (N.M. Gupta).

0926-3373/$ – see front matter © 2004 Elsevier B.V. All rights reserved.
doi:10.1016/j.apcatb.2004.07.001

molecules such as carbon monoxide and methanol, where the bulk oxygen of uranium oxide played a vital role [18]. In continuation of these previous studies, we have now exploited the visible region absorbance ($\lambda > 380$ nm) of anchored uranyl ions for the vapor-phase photooxidation of organic substrates in heterogeneous mode. The objective of the present investigation was to demonstrate the effectiveness of uranyl-containing MCM-41 mesoporous host as a photocatalyst for the complete destruction of typical volatile organic compounds (VOCs), such as methanol, in the presence of solar radiation. In order to enable a comparison, parallel experiments were performed to monitor the photocatalytic behavior of TiO_2. The catalytic reaction of methanol at elevated temperatures but in the absence of solar radiation was also monitored so as to discriminate between the photo- and thermal radiation induced processes. In situ fluorescence and EPR studies were carried out under identical conditions in order to examine the oxidation state of uranium during the photocatalytic process. Also, in situ FTIR spectroscopy was employed for monitoring of the transient species formed over uranyl-anchored MCM-41 on exposure to methanol, without and under visible light. An attempt is also made in this study to delineate the reaction routes involved and to identify the role of uranyl ions (UO_2^{2+}) in the photocatalytic oxidation of methanol.

2. Experimental

2.1. Catalyst preparation and characterization

The uranyl-anchored MCM-41 catalyst was prepared and characterized, as per the procedures described elsewhere [16,17]. A direct template exchange process was employed for this purpose wherein a 0.005 M uranyl nitrate precursor solution adjusted at pH of 5.0 was exchanged with surfactant cations in the as-synthesized MCM-41 molecular sieve for a period of 12 h. The sample, after drying at ~70 °C, was calcined at 550 °C for 2 h in N_2 and 6 h in air, and is designated as UO_2^{2+}/MCM-41 in the text. The uranium content of this sample, analyzed by ICP-AES, was found to be 9.8 wt.%. The BET surface area and pore diameter of UO_2^{2+}/MCM-41 was found to be ~600 $m^2\,g^{-1}$ and 28 Å, respectively; the corresponding values in the case of the parent MCM-41 subjected to similar pretreatments being around 1000 $m^2\,g^{-1}$ and 30 Å, respectively. The XRD pattern of UO_2^{2+}/MCM-41 exhibited reflections characteristic of hexagonal MCM-41 structure, indicating the integrity of the structure in guest–host system [16]. At higher 2θ values, weak reflections appearing at d = 4.15, 3.39, 2.62, 2.07, 1.96, and 1.75 Å indicated the presence of α-U_3O_8 moieties encapsulated in the mesopores of MCM-41 [17,18].

The anchoring of uranyl ions to the defect sites of the silicate matrix was established with the help of fluorescence, DRUV-VIS, and FTIR spectroscopic techniques [16,17], as is described in a later section in brief.

2.2. Catalytic activity measurements

The room-temperature reaction of methanol (0.26–7.8 vol.%) in air was carried out over the catalyst in static mode and in the presence of direct solar radiation. Two different catalytic reactors were employed for this purpose: one made of pyrex glass and another of quartz. Both the reaction cells were dimensionally identical (15 mm diameter, 150 mm length), and were sealed at the top with the help of a rubber septum. About 100 mg batch of a catalyst sample was dispersed uniformly in the reaction cell and was degassed appropriately before introduction of the reactants. The final pressure was kept at around 1.2 bar. Experiments were also conducted in the absence of solar radiation but at elevated reaction temperatures, so as to evaluate the thermal activity of the catalyst. A Chemito model-8510 gas chromatograph, equipped with thermal conductivity detector (set at 120 °C) and Porapak-Q (100 °C), or alternatively a Sperocarb (100 °C) column was employed for analysis of reactants and products.

The average photon flux of sunlight, as measured by uranyl oxalate actinometry [21], was found to be ~3.1×10^{14} and 2.9×10^{14} photons/s/cm^2 using the quartz and pyrex cells, respectively.

2.3. Spectroscopy studies

EPR spectra were recorded (Bruker ESP 300 X-band spectrometer operating at 9–9.6 GHz, magnetic field modulation at 100 KHz) at 6 db, 60 mW power, and at different temperatures in the range 100–300 K. A dual cavity system was employed for g-value calibration, using DPPH (g_e = 2.0036) as standard. About 10 mg sample placed in a pyrex tube assembly fitted with greaseless joints and stopcocks was exposed to methanol (7.8% v/v in N_2) under inert atmosphere, subjected to irradiation from a 400 W medium pressure mercury lamp (model 3040, type PM 135, serial no. H184, Applied Photophysics Ltd., UK) with a photon flux = 6.5×10^{14} photons/s/cm^2 for 2 h, and stored immediately in liquid nitrogen.

Fluorescence measurements were made on a LS-55 Perkin-Elmer spectrofluorimeter. For in situ studies, the equipment required consisted of triangular quartz cell (1 cm × 1 cm) fitted with an appropriate septum arrangement. Around 100 mg catalyst pretreated at 100 °C for 1 h was placed in the quartz cell and was evacuated prior to introduction of methanol vapor (7.8% v/v in air). A xenon lamp (λ_{ex} = 310 nm) served as a radiation source. The fluorescence intensity was measured every half an hour. Similar experiments were also carried out in the absence of methanol.

In situ FTIR spectra of UO_2^{2+}/MCM-41 and corresponding pristine siliceous MCM-41 samples were recorded in transmission mode using a high-temperature and high-pressure stainless steel cell, prior to and after dosing methanol at room temperature. An appropriate arrangement

was made for exposure of the sample to visible light by fixing a small size 50-W incandescent light source inside the IR cell. This helped in the in situ monitoring of the transient species, without and in the presence of radiation. A self-supporting sample wafer weighing ~100 mg was evacuated for 3–4 h at 10^{-3} Torr, prior to dosing of methanol vapor (7.8% v/v) + air. A JASCO FTIR-610 spectrometer equipped with a DTGS detector was employed, and 300 scans were collected at a resolution of 4 cm^{-1} for recording each spectrum. The values given in parentheses in some of the figures represent the absorbance values of particular IR bands and serve as an estimate of their relative intensity. Methanol of Analytical reagent grade (SISCO Research Laboratories, Mumbai, India) was purified by distillation before use.

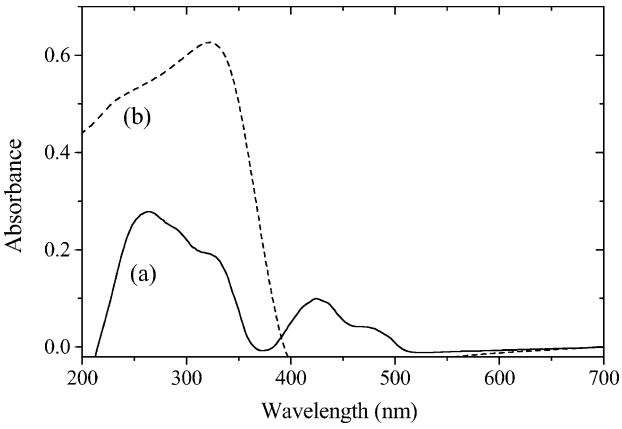

Fig. 2. Comparative absorbance spectra of (a) UO_2^{2+}/MCM-41 and (b) TiO_2.

3. Results and discussion

3.1. The mode of uranyl binding onto the silicate matrix

Fig. 1 presents the typical fluorescence spectra of uranyl-exchanged MCM-41 before (curve (a)) and after calcination at 550 °C (curve (b)). For comparison, the fluorescence spectrum of uranyl nitrate is shown in the inset of this figure. We observe overlapping and broad fluorescence bands in Fig. 1a in place of well-defined and sharp emission bands of uranyl nitrate in the 450–600 nm range (Fig. 1, inset), which are assigned to transitions between the vibrational level of first excited electronic state ($\nu' = 0$) to the vibrational levels of ground electronic state ($\nu'' = 0$–5) of uranyl ions [22]. Apart from this, all the band positions are found to be shifted to a higher wavelength, which is an indication of weakening of the uranyl (O=U=O) linkages. These observations are indicative of an interaction of UO_2^{2+} ions with the silicate (≡Si–O^- groups) matrix, as is discussed elsewhere in detail [16,17]. A decrease in the intensity of emission bands after calcination (curve (b)) is consistent with the XRD data, suggesting the transformation of some of the UO_2^{2+} species to non-fluorescent uranium oxides [17,18].

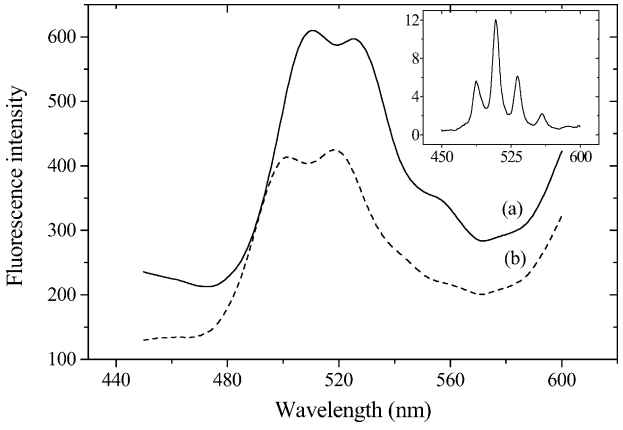

Fig. 1. Fluorescence spectra of (a) uranyl-exchanged MCM-41 and (b) uranyl-anchored MCM-41. The inset shows fluorescence spectrum of uranyl nitrate dihydrate.

Curve (a) in Fig. 2 shows the DRUV-VIS spectrum of UO_2^{2+}/MCM-41 sample. As in the case of Fig. 1, the DRUV-VIS spectrum of uranyl-anchored MCM-41 comprises of broad and overlapping bands instead of sharp bands in uranyl nitrate spectrum, arising due to definite transitions from electronic levels coupled to O=U=O vibrations [23]. This again may be attributed to the bonding of ≡Si–O^- units to linear O=U=O molecules in the equatorial plane forming a uranate type of local structure [16,17]. FTIR study similarly provided evidence for the strong binding of uranyl group, $[O=U=O]^{2+}$ with the ≡Si–O^- sites of the MCM-41 matrix [15]. Thermogravimetric-differential thermal analysis of UO_2^{2+}/MCM-41 exhibited a single weight loss of ~18% and a corresponding endothermic peak at ~370 K, attributed to the release of adsorbed water or weakly coordinated hydroxyl groups. On the basis of above information and in consideration of the stability requirement of a coordination structure, the uranyl groups can be envisaged to be anchored to the silicate matrix as follows (Scheme 1).

3.2. Absorbance spectra of UO_2^{2+}/MCM-41 versus TiO_2

Fig. 2b shows the comparative DRUV-VIS spectrum of a TiO_2 (anatase, surface area, 12 $m^2\,g^{-1}$) sample. As mentioned above, the absorbance of UO_2^{2+}/MCM-41 shows weak bands between 330 and 500 nm and progressively stronger bands towards the ultraviolet region. The absorbance region of 200–500 nm in Fig. 2a matches with that of

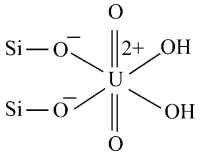

Scheme 1. Uranyl-anchored MCM-41 catalyst UO_2^{2+}/MCM-41.

the isolated uranyl groups in aqueous medium. It is reported that the spectra of a large number of uranyl complexes are virtually independent of the chemical nature of the ligand, but are strongly dependent of the total symmetry of the complex [3]. The change in the relative intensity of various absorbance bands in Fig. 2a as compared to that of the uranyl groups in aqueous phase (see [3]) is thus a clear evidence of these groups being in a constrained environment because of their immobilization. Further, as is evident from the data in Fig. 2a, the absorbance component of UO_2^{2+}/MCM-41 in visible region would make it an ideal photocatalyst for applications in sunlight, compared to a TiO_2 photocatalyst with its absorbance mainly in the ultraviolet region (Fig. 2b).

3.3. Photocatalytic activity

Shown in Fig. 3 is the photocatalytic activity of UO_2^{2+}/MCM-41 for the room temperature oxidation of methanol at its varying concentrations in air, measured in a quartz reaction cell in the presence of sunlight. No unreacted methanol was observed under present experimental conditions, indicating its complete adsorption/reaction over the catalyst. The only products obtained were CO_2 and water, though no attempt was made for quantitative estimation of the latter. As seen in data of Fig. 3, the reaction progress depended upon methanol concentration, and 100% conversion to CO_2 was achieved within about 30 min time in case of 0.26 vol.% methanol concentration in air (Fig. 3a). Even though the overall CO_2 yield was higher in the experiments conducted with higher methanol concentrations in air, the product yield in terms of percentage conversion was lower. Therefore, a longer duration of exposure was needed in such cases so as to achieve a 100% conversion to CO_2 as depicted in curves (b)–(d) of Fig. 3. This observation suggests that the availability of uranyl ions at a particular stage may control the overall progress of the reaction.

No formation of CO_2 was observed in the parallel experiments when performed on uranyl-free MCM-41 sample, even though a considerable amount of reactant methanol was found to be adsorbed. Similarly, no formation of CO_2 was observed in room-temperature reaction of methanol over UO_2^{2+}/MCM-41 in the absence of radiation. We also confirmed that the photolysis of methanol did not occur in gas phase, i.e. in the absence of a catalyst. Furthermore, experiments carried out using bulk α-U_3O_8 as a catalyst under identical conditions did not result in the measurable formation of CO_2. These results thus clearly provide an evidence of the crucial role played by the highly dispersed uranyl ions in the studied photocatalytic process.

Fig. 4 presents the corresponding data on photocatalytic oxidation of methanol in the exclusive presence of visible-region radiation, collected using a pyrex glass cell under identical reaction conditions. It can be seen that compared to the results of Fig. 3, the conversion rates were lower when the reaction was carried out in a pyrex cell, the effect being more pronounced for higher concentrations of reactant methanol in air (see Fig. 4c and d). Thus, at the lower concentrations of methanol (<1.3 vol.%) in air (Fig. 4a and b), almost complete conversion of methanol was achieved under visible radiation, although after a longer radiation exposure compared to that shown in Fig. 3. For instance, with 0.26% concentration of methanol in air, 100% conversion to form CO_2 was observed after 30 and 90 min of irradiation time, when the reaction was carried out in the cells made of quartz and pyrex glass, respectively. These results thus confirm that the UO_2^{2+}/MCM-41 sample is active for both the visible and UV region radiation, even though the overall yield may depend upon the wavelength. The dependence of this photocatalytic process on the wavelength of incident radiation is being further investigated in our laboratory. Meanwhile, the present results are significant and confirm that the uranyl ions anchored in mesopores of MCM-41 indeed behave as visible light photocatalysts.

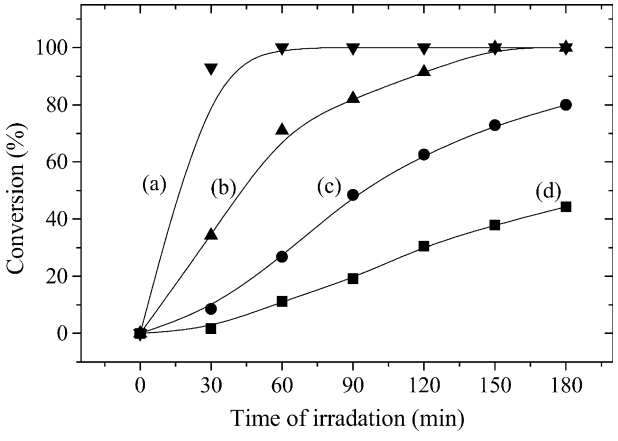

Fig. 3. Time-dependent variation in CO_2 yield during oxidation of methanol in air over UO_2^{2+}/MCM-41 under irradiation in sunlight in a quartz cell. Curves (a)–(d) represent methanol concentrations in air varying at 0.26, 1.3, 3.4, and 7.8 vol.%, respectively.

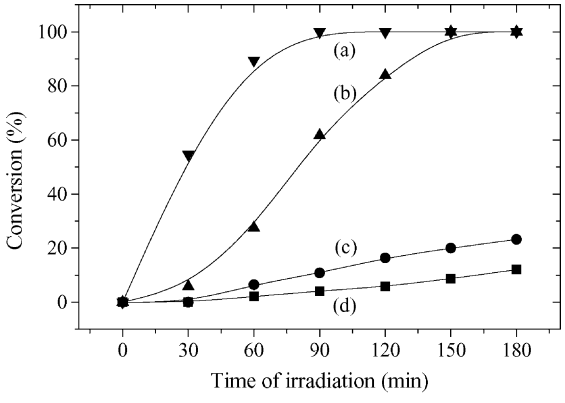

Fig. 4. Time-dependent variation in CO_2 yield during oxidation of methanol in air over UO_2^{2+}/MCM-41 under irradiation in sunlight in a pyrex cell. Curves (a)–(d) represent methanol concentrations in air varying at 0.26, 1.3, 3.4, and 7.8 vol.%, respectively.

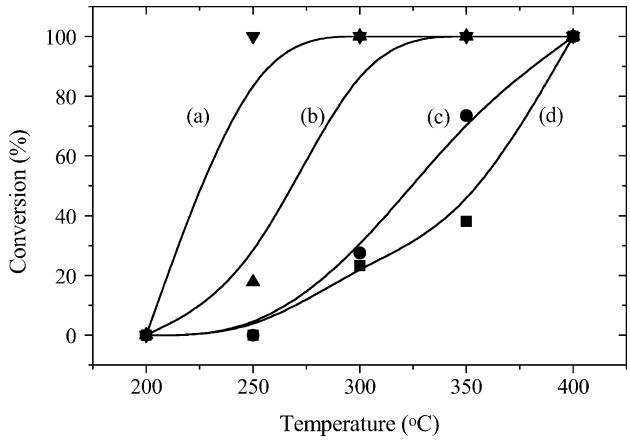

Fig. 5. Temperature-dependent variations in CO_2 yield during oxidation of methanol in air over UO_2^{2+}/MCM-41 in the absence of irradiation. Curves (a)–(d) represent methanol concentrations in air varying at 0.26, 1.3, 3.4, and 7.8 vol.%, respectively.

Fig. 5 presents data on the temperature-dependent catalytic activity of UO_2^{2+}/MCM-41 for oxidation of methanol in the absence of radiation. It can be seen that the formation of products, viz., CO_2, begins only at ~250 °C for lower concentrations of methanol in air and at around 300 °C for higher concentrations. As reported by us earlier [17,18], the presence of UO_X moieties in the mesopores of MCM-41 and MCM-48 are responsible for this catalytic oxidation of methanol, where the involvement of lattice oxygen plays a vital role. A number of studies reported by other authors similarly report that the supported oxides of uranium are active for the destruction of VOCs at temperatures above 350 °C [24–27]. In that respect, it is apparent that the room-temperature photocatalytic oxidation over UO_2^{2+}/MCM-41 (Figs. 3 and 4) has an edge over the conventional catalytic combustion, in that it effects the complete oxidation under the ambient conditions of sunlight and air.

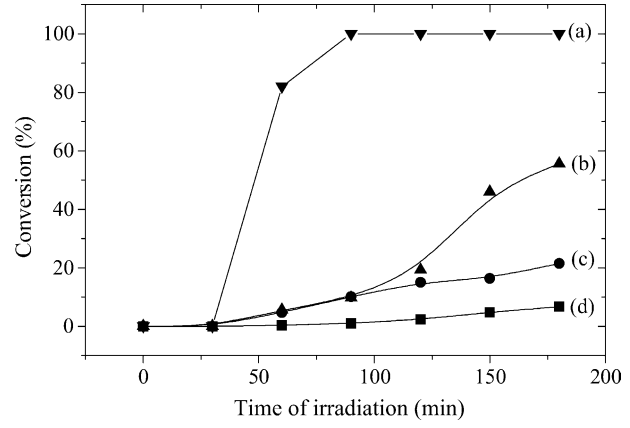

Fig. 6. Time-dependent variation in CO_2 yield during oxidation of methanol in air over TiO_2 under irradiation in sunlight in quartz cell. Curves (a)–(d) represent methanol concentrations in air varying at 0.26, 1.3, 3.4, and 7.8 vol.%, respectively.

Fig. 6 gives the comparative data on photooxidation of methanol over TiO_2 catalyst, when measured in a quartz cell. As seen from a comparison of Figs. 3 and 6, the UO_2^{2+}/MCM-41 is much more effective in terms of the time-dependent rate of oxidation of methanol as compared to bulk TiO_2. For instance, while 100% $CH_3OH \rightarrow CO_2$ conversion took place in less than 30 min using UO_2^{2+}/MCM-41 (Fig. 3a) for methanol concentration feed at 0.26 vol.%, the corresponding time in the case of TiO_2 was around 90 min (Fig. 6a). A similar trend is noticed in curves (b)–(d) of these figures for higher concentrations of methanol in air. It is also of interest to notice that while the reaction is almost instantaneous in case of results in Fig. 3, there is an induction period of about 30 min in case of the data in Fig. 6.

Based on the results presented in Figs. 3 and 6, we surmise that the more efficient and fast response photocatalytic behavior exhibited by UO_2^{2+}/MCM-41 vis-à-vis TiO_2 may arise not only because of the visible region absorbance of the former but also because of the two distinct mechanistic routes followed. Thus, as is well documented, the TiO_2 photocatalyzed oxidation proceeds via electron hole pairs generated upon UV-induced band gap excitation, where electrons or holes interact with reactant molecules to form molecular or ionic radicals in excited state that undergo molecular transformation leading thereby to product formation. The quantum efficiency of this process depends upon various possible recombination modes of these species, the details of which are described in literature [28]. In the case of uranyl groups, an electron transfer from methanol molecule to photo-excited UO_2^{2+} (i.e. $^*UO_2^{2+}$) would lead to the formation of a U(V)-molecule radical cation complex [3]. The deprotonation within the radical pair will give rise to formation of methoxyl radical resulting eventually in its decomposition/oxidation. The efficiency of this overall electron transfer process between the excited uranyl ion and methanol molecule, or for that matter any other organic molecule, is expected to be close to 100%. This explains the instantaneous and the high photocatalytic activity of UO_2^{2+}/MCM-41 as demonstrated in Fig. 3.

3.4. *In situ* EPR and fluorescence studies

In the sections that follow, we describe the results of in situ fluorescence and EPR studies that help in establishing the valence fluctuation of uranium during the photocatalytic oxidation of methanol.

Curves (a)–(e) in Fig. 7 depict the EPR spectra of UO_2^{2+}/MCM-41 under the various conditions of radiation exposure. As observed in Fig. 7a, the irradiated catalyst did not show EPR signal in the absence of methanol except for a broad background. When the sample was exposed to methanol vapor followed by irradiation, a highly symmetric EPR signal at a g-value of 1.65 was observed, and this signal was found to be stable on raising the sample temperature to

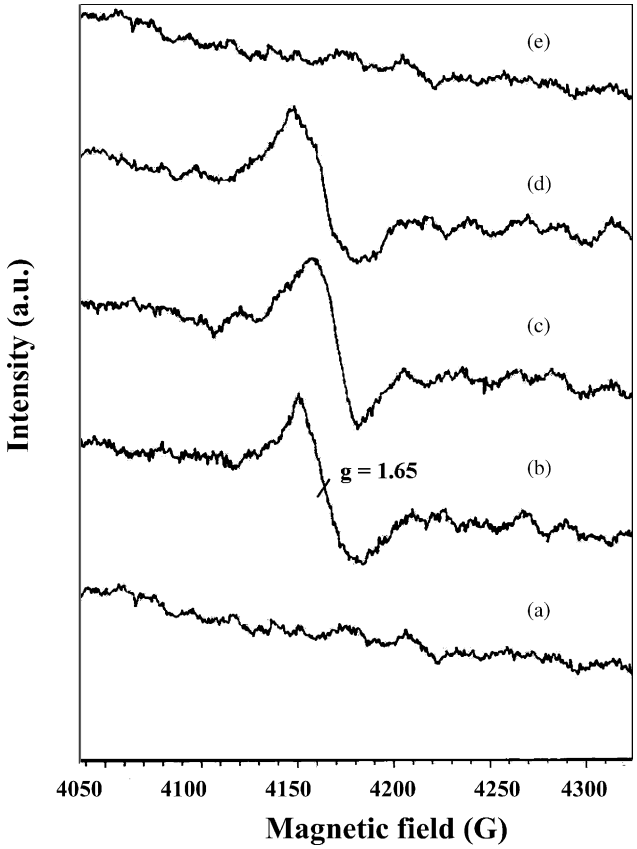

Fig. 7. EPR spectra of UO_2^{2+}/MCM-41 irradiated for 2 h in visible light in the presence of methanol (7.8 vol.%) under an inert atmosphere. (a) No methanol, (b–d) recorded in the presence of methanol at different sample temperatures of 100, 200, and 300 K, respectively, (e) sample in (d) exposed to atmosphere.

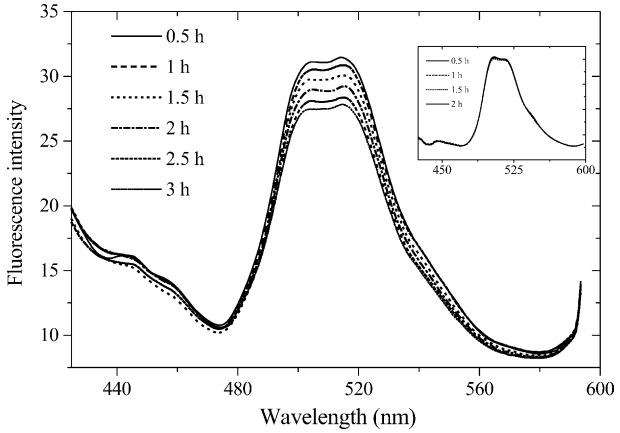

Fig. 8. Decrease in intensity of fluorescence spectra of UO_2^{2+}/MCM-41 in the presence of methanol vapor monitored as a function of irradiation time. The inset shows the fluorescence spectra of UO_2^{2+}/MCM-41 in the absence of methanol vapor.

300 K (Fig. 7b–d). Subsequent exposure to air resulted in the disappearance of the EPR signal (Fig. 7e).

It is well documented that the uranium exhibits an EPR signal in its trivalent [U(III)] and pentavalent [U(V)] oxidation states. U(III), however, is known to give a multiplet signal with g_x, g_y, and g_z components due to lifting of degeneracy of the f^3 configuration [29]. On the other hand, the magnetic properties of U(V) are known to differ with the nature of the compound, the crystal field interaction of the matrix material, and the interaction with neighbouring atoms, with g-value of the EPR signal being reported to range from 1.25 to 2 [29]. Therefore, the EPR signal in Fig. 7 could be attributed to the 5+ oxidation state of uranium, produced due to photo-induced electron transfer from methanol to $^*UO_2^{2+}$. The disappearance of the signal on exposure to air (Fig. 7e) confirms the reversible and active participation of U(VI) as active sites.

The participation of uranyl ions in the photocatalytic process was also corroborated by the fluorescence spectra of UO_2^{2+}/MCM-41 catalyst. Fig. 8 shows in situ fluorescence spectra of UO_2^{2+}/MCM-41 in the presence of methanol vapor (7.8% v/v in air), which exhibits a gradual decrease in intensity when monitored as a function of irradiation time. Since the uranyl ions in 6+ valence state are the only form of uranium that fluoresce [22], the observed decrease in intensity provides an evidence of U(VI) → U(V) transformation as a result of photoexcitation. We may mention that no such intensity change was detected when the fluorescence spectra of UO_2^{2+}/MCM-41 were recorded in the absence of methanol, as shown in the representative data included in the inset of Fig. 8. These results thus confirm the lowering of the oxidation state of U(VI), because of the electron transfer from methanol molecules.

3.5. In situ FTIR study of surface adsorbed species

Fig. 9 exhibits the prominent IR bands in stretching and deformation regions, when UO_2^{2+}/MCM-41 sample was exposed to methanol vapor (7.8 vol.%) + air at room temperature, prior to (curve (a)) and after 5 min exposure to visible radiation (curve (b)). Spectrum (c) was plotted after post-irradiation evacuation of the sample. The corresponding vibrational bands formed over uranium-free MCM-41 sample on exposure to CH_3OH are depicted in Fig. 10. In the following, we discuss some salient features of these IR results.

(i) IR spectra of Fig. 9a and Fig. 10a exhibit that a large amount of methanol gets adsorbed over UO_2^{2+}/MCM-41 and siliceous MCM-41 samples, as seen from the strong bands in the 3500–2000 cm^{-1} and 1800–1275 cm^{-1} regions, even though the nature of binding and the amount adsorbed were different. This becomes apparent since the υ(OH) band of adsorbed methanol appears at different frequencies, i.e. at 3207 cm^{-1} in case of MCM-41 (Fig. 10a) and at 3178 cm^{-1} for UO_2^{2+}/MCM-41 (Fig. 9a), indicating the stronger adsorption of methanol and hence the weakening of O–H bonding in case of U-containing sample. The weak bands appearing at around 3002 and 2922 cm^{-1} in these figures may be identified with the asymmetric and symmetric C–H

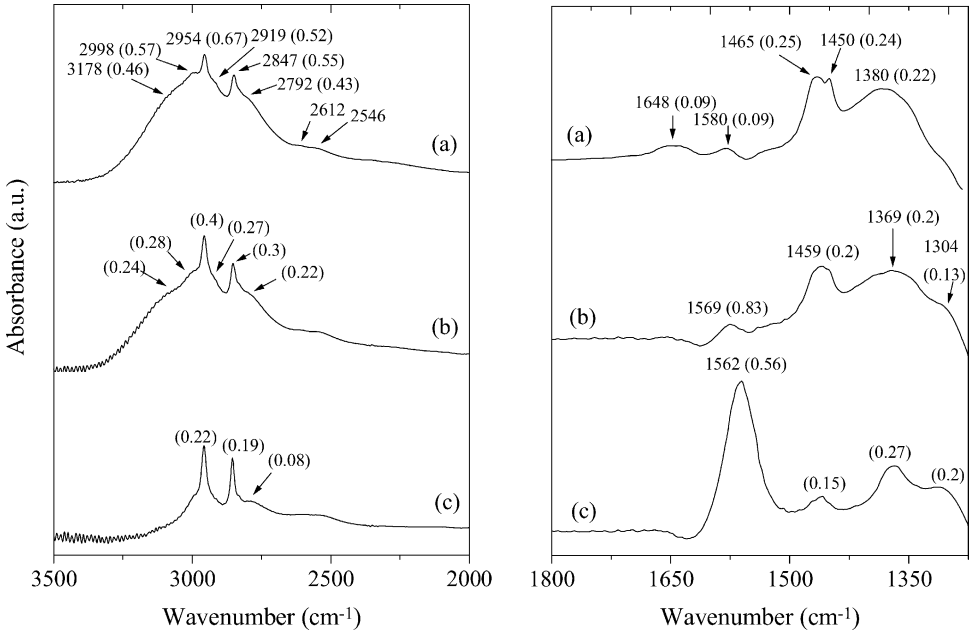

Fig. 9. In situ FTIR spectra of UO_2^{2+}/MCM-41 with methanol in the absence of irradiation at room temperature for (a) 5 min, and in the presence of irradiation for (b) 5 min (e) post-radiation evacuation for 5 min.

stretching vibrations of adsorbed methanol. The assignment of these bands is validated by their instant removal on evacuation (curve (c), Figs. 9 and 10) [30].

The prominent IR bands observed at ~2954 and 2847 cm^{-1} and a shoulder at ~2818 cm^{-1} in Fig. 9a and Fig. 10a may be assigned to $\upsilon_{as}(CH_3)$, $\upsilon_s(CH_3)$, and $2\delta_s(CH_3)$ vibrations of widely reported methoxy groups [30–40], bonded to the framework silanol groups of the host matrix (i.e. ≡Si–OCH_3). In the corresponding deformation region, $\delta_{as}(CH_3)$ and $\delta_s(CH_3)$ vibrations of (Si–OCH_3 give rise to bands at ~1466 and 1450 cm^{-1} (Fig. 9a and Fig. 10a).

The additional bands observed in Fig. 9a at ~2792 and ~2612 cm^{-1} (seen more clearly in the deconvoluted spectrum) could be attributed to the asymmetric and symmetric C–H stretching of methoxy groups bonded to uranium, i.e. U–OCH_3, since these bands were not observed

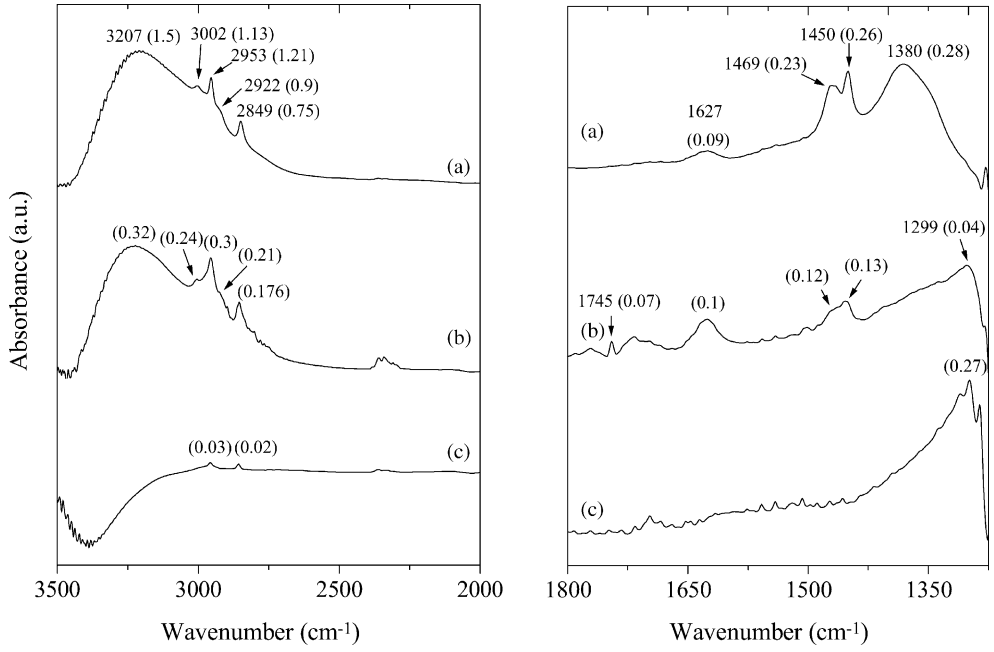

Fig. 10. In situ FTIR spectra of MCM-41 with methanol in the absence of irradiation at room temperature for (a) 5 min, and in the presence of irradiation for (b) 5 min (e) post-radiation evacuation for 5 min.

in the case of siliceous MCM-41 sample (see Fig. 10a), as is also reported before [41].

Further, weak band at ~2542 cm^{-1} was observed only for adsorption of methanol over UO_2^{2+}/MCM-41 (Fig. 9a) and not on U-free sample (Fig. 10a). This band is characteristic of 2δ(CH) vibrations of the formate group [30], and their formation has been reported earlier in adsorption of methanol over uranium oxides at room temperature [41] and also on various other metal oxide systems at elevated temperatures [30,31,40]. Other bands due to the formate group such as $\upsilon_{as}(CO_2)$ + δ(CH), and υ(CH) are masked by the bands due to methoxy groups and adsorbed methanol and hence are not seen clearly. The corresponding deformation region bands are however, observed at ~1580 and 1375 cm^{-1} (broad band) corresponding to $\upsilon_{as}(COO^-)$, $\delta(CH_2)$, and $\upsilon_s(COO^-)$ vibrations of formate group. Further, the band at ~1375 cm^{-1} could also be attributed to the δ(COH) of the adsorbed, undissociated methanol [30]. In siliceous MCM-41, the formation of formate species was not observed, as seen in Fig. 10a.

(ii) Various changes were noticed in the above-mentioned vibrational bands when the samples were subjected to visible light irradiation following adsorption of methanol. For instance, the formation of new bands at ~1570 and 1368–1300 cm^{-1} was observed only in case of UO_2^{2+}/MCM-41 sample (Fig. 9b), and the intensity of these bands increased with the increasing radiation dose as measured by their absorbance value. These bands are assigned to $\upsilon_{as}(COO^-)$, $\delta(CH_2)$, and $\upsilon_s(COO^-)$ vibrations of the formate groups attached to uranium [31,32,40]; and the growth in their concentration as a function of radiation dose is depicted in Fig. 11. No such bands were formed in the case of pristine MCM-41 (Fig. 10b), thus indicating that uranyl sites are solely responsible for this photocatalytic process.

(iii) The methoxy groups ((Si–OCH_3) were found to be rather stable and were detectable even after long duration of irradiation.

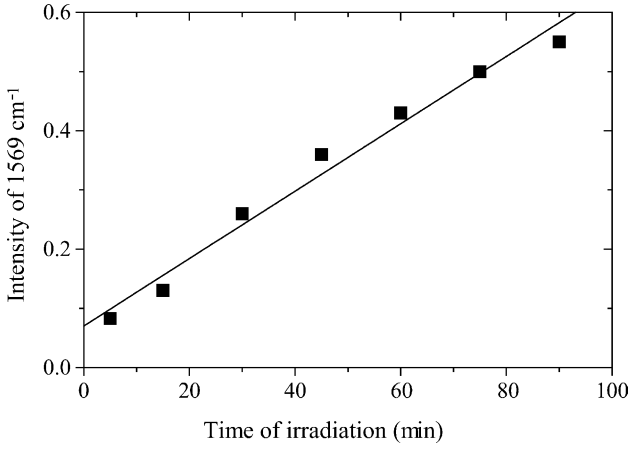

Fig. 11. Plot of intensity of band at 1569 cm^{-1} with respect to irradiation time.

We may thus conclude that the silanol groups of MCM-41 and the excited uranyl groups anchored on to the walls serve as independent adsorption sites for methanol molecules. Since no photooxidation of methanol occured in case of U-free MCM sample, it is surmised that the ≡Si–OCH_3 groups may play no significant part in the photocatalytic process. On the contrary, the molecules adsorbed at the $^*UO_2^{2+}$ sites may undergo oxidation reaction via the formation of the above described formate-type species in the presence of radiation. The active and reversible participation of uranyl groups in this photocatalytic process occurs via formation of U(V) or UO_2^{2+} species, as is established clearly by the in situ EPR and fluorescence spectroscopy investigations.

Based on the observations described above, we infer that the hydrogen abstraction by $^*UO_2^{2+}$ leads to the formation of a carbon centred radical, which is accompanied by the reduction of UO_2^{2+} to UO_2^+, as observed by EPR and fluorescence spectroscopy study. The carbon centred radical

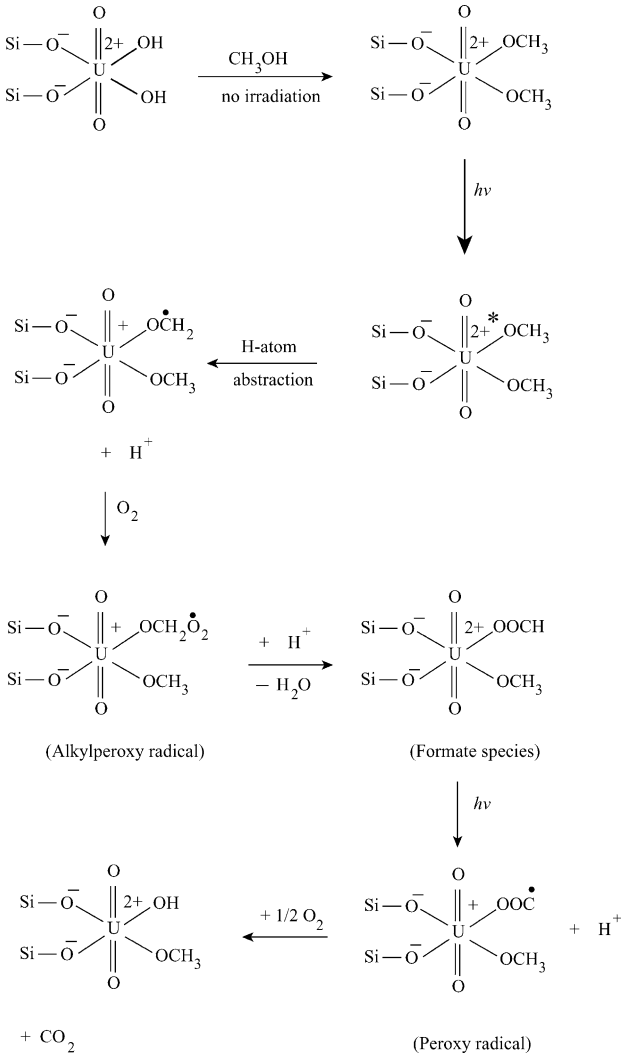

Scheme 2. Reaction mechanism of photooxidation of methanol over UO_2^{2+}/MCM-41.

in turn may react with oxygen to form an alkylperoxy complex, which in turn reacts with UO_2^+ to give rise to formate-type species (Fig. 9). The formate species may ultimately lead to carbon dioxide formation under the higher flux of irradiation.

In summary, the reaction steps that may occur on UO_2^{2+}/MCM-41 during the interaction of methanol at room temperature, without and in the presence of radiation may be identified as follows.

3.5.1. Reaction occurring at framework silanol sites

Silanol groups interact with methanol to form stable methoxy groups, i.e.

$$\equiv Si-OH \underset{CH_3OH}{\longrightarrow} \equiv Si-OCH_3$$

3.5.2. Reactions occurring at uranyl groups

Various redox transformations that may occur over UO_2^{2+}/MCM-41 as a result of sunlight irradiation following methanol adsorption at uranyl sites may be represented by the following reaction routes (Scheme 2).

4. Conclusions

In the present study, we have demonstrated for the first time that the thermally stable uranyl ions anchored within the mesoporous MCM-41 matrix may serve as highly efficient photocatalysts in the complete oxidation of methanol, a typical VOC, under the conditions of relevance for treatment of industrial effluents. The photocatalytic activity was determined under the presence of ambient sunlight and was found to be high even under conditions where only the visible part of sunlight was available ($\lambda >$ 400 nm). This proves that the uranyl-anchored MCM-41 behave as a true 'visible light' photocatalyst. The UO_2^{2+}/MCM-41 samples were found to be more efficient under solar radiation as compared to a TiO_2 photocatalyst in terms of photon efficiency. This is attributed to not only the difference in the absorbance, but also to the different mechanistic routes followed.

In situ EPR and fluorescence studies revealed that U(VI) or UO_2^{2+} in its excited state is an active and reversible participant in the photocatalytic process. Further, with the help of in situ FTIR technique, we were able to monitor some of the intermediate species formed over the catalyst surface. These studies revealed that certain formate-type species were produced at uranyl sites in the presence of radiation and resulted ultimately in the formation of CO_2.

Acknowledgements

We gratefully acknowledge Dr. Kamal Kishore, Radiation Chemistry and Chemical Dynamics Division, for valued suggestions and comments. We thank Dr. R.D. Saini in setting up the photocatalysis equipment and Dr. R.M. Kadam, Radiochemistry Division, for EPR results. The authors also thank Dr. A. Datta, IIT-Bombay, for assistance in recording in situ fluorescence spectra. This work was performed under BRNS Contract No. 99/37/BRNS/1049.

References

[1] E. Rabinowitch, R.L. Belford, Spectroscopy and Photochemistry of Uranyl Compounds, Pergamon Press, Oxford, 1964.
[2] V. Balzani, F. Bolletta, M.T. Gandolfi, M. Maestri, Top. Curr. Chem. 75 (1978) 1.
[3] H.D. Burrows, T.J. Kemp, Chem. Soc. Rev. 3 (1974) 139.
[4] W.-D. Wang, A. Bakac, J.H. Espenson, Inorg. Chem. 34 (1995) 6034.
[5] W.-D. Wang, J.H. Espenson, Inorg. Chem. 34 (1995) 4049.
[6] Y. Mao, A. Bakac, Inorg. Chem. 35 (1996) 3925.
[7] Y. Mao, A. Bakac, J. Phys. Chem. 100 (1996) 4219.
[8] T.M. McCleskey, C.J. Burns, W. Tumas, Inorg. Chem. 38 (1999) 5924.
[9] T.M. Bergfeldt, W.L. Waltz, X. Xu, P. Sedlak, U. Dreyer, H. Mockel, J. Lilie, J.W. Stephenson, Can. J. Chem. 81 (2003) 219.
[10] M. Sarakha, M. Bolte, H.D. Burrows, J. Phys. Chem. A 104 (2000) 3142.
[11] M. Sarakha, M. Bolte, H.D. Burrows, J. Photochem. Photobiol. A: Chem. 107 (1997) 101.
[12] S.L. Suib, A. Kostapapus, D.J. Psaras, J. Am. Chem. Soc. 106 (1984) 1614.
[13] S.L. Suib, K.A. Carrado, Inorg. Chem. 24 (1985) 863.
[14] S.L. Suib, J.F. Tanguay, M.L. Occelli, J. Am. Chem. Soc. 108 (1986) 6972.
[15] S. Dai, D.H. Metcalf, G.D. Del Cul, L.M. Toth, Inorg. Chem. 35 (1996) 7786.
[16] K. Vidya, S.E. Dapurkar, P. Selvam, S.K. Badamali, N.M. Gupta, Micropor. Mesopor. Mater. 50 (2001) 173.
[17] K. Vidya, S.E. Dapurkar, P. Selvam, S.K. Badamali, D. Kumar, N.M. Gupta, J. Mol. Catal. A: Chem. 181 (2002) 91, 191 (2003) 149.
[18] D. Kumar, V.S. Kamble, N.M. Gupta, Catal. Lett. 88 (2003) 175.
[19] D. Kumar, S. Bera, A.K. Tripathi, G.K. Dey, N.M. Gupta, Micropor. Mesopor. Mater. 66 (2003) 157.
[20] D. Kumar, K.T. Pillai, V. Sudersanan, G.K. Dey, N.M. Gupta, Chem. Mater. 15 (2003) 3859.
[21] G.L. Wesley, G.S. Forbes, J. Am. Chem. Soc. 52 (1930) 3139.
[22] G.H. Dieke, A.B.F. Duncan, in: Spectroscopic Properties of Uranium Compounds, McGraw Hill Book Company, Inc., 1949.
[23] S.P. McGlynn, J.K. Smith, J. Mol. Spectr. 6 (1964) 164.
[24] G.J. Hutchings, C.S. Heneghan, I.D. Hudson, S.H. Taylor, Nature 384 (1996) 341.
[25] C.S. Heneghan, G.J. Hutchings, S.R. O'Leary, S.H. Taylor, V.J. Boyd, I.D. Hudson, Catal. Today 54 (1999) 3.
[26] S.H. Taylor, C.S. Heneghan, G.J. Hutchings, I.D. Hudson, Catal. Today 59 (2000) 249.
[27] S.H. Taylor, S.R. O'Leary, Appl. Catal. B 25 (2000) 137.
[28] M.A. Fox, M.T. Dulay, Chem. Rev. 93 (1993) 341.
[29] I. Ursu, V. Lupei, Bull. Magn. Reson. 6 (1984) 162.
[30] G. Busca, A.S. Elmi, P. Forzatti, J. Phys. Chem. 91 (1987) 5263.
[31] I.A. Fisher, A.T. Bell, J. Catal. 184 (1999) 357.
[32] D.B. Clarke, D.K. Lee, M.J. Sandoval, A.T. Bell, J. Catal. 150 (1994) 81.
[33] G.J. Millar, C.H. Rochester, K.C. Waugh, J. Chem. Soc., Faraday Trans. 87 (1991) 2785.
[34] T.R. Forester, R.F. Howe, J. Am. Chem. Soc. 109 (1987) 5263.

[35] M.T. Aronson, R.J. Gorte, W.E. Fameth, J. Catal. 105 (1987) 455.
[36] G. Mirth, J.A. Lercher, M.W. Anderson, J. Klinowski, J. Chem. Soc., Faraday Trans. 86 (1990) 3839.
[37] J. Nováková, L. Kubelková, Z. Dolejšek, J. Catal. 108 (1987) 208.
[38] L. Kubelková, J. Nováková, K. Nedomová, J. Catal. 124 (1990) 441.
[39] C. Flego, A. Carati, C. Perego, Micropor. Mesopor. Mater. 44 (2001) 733.
[40] V. Lochař, J. Machek, J. Tichý, Appl. Catal. A: Gen. 228 (2002) 95.
[41] D. Kumar, V.S. Kamble, N.M. Gupta, Catal. Lett. 88 (2003) 175.